Conformational dynamics of the membrane enzyme LspA upon antibiotic and substrate binding

T. Caldwell, O. Vickery, J. Colburn, P. Stansfeld, L. Columbus

Abstract

Lipoprotein signal peptidase (LspA) is an aspartyl protease that cleaves the transmembrane helix signal peptide of lipoproteins as part of the lipoprotein processing pathway. Members of this pathway are excellent targets for the development of antibiotic therapeutics because they are essential in Gram-negative bacteria, are important for virulence in Gram-positive bacteria, and may not develop antibiotic resistance. Here we report the conformational dynamics of LspA in the apo state and bound to the antibiotic globomycin determined using MD simulations and EPR. The periplasmic helix fluctuates on the nanosecond timescale and samples unique conformations in the different states. In the apo state, the dominant conformation is the most closed and occludes the charged active site from the lipid bilayer. With antibiotic bound there are multiple binding modes with the dominant conformation of the periplasmic helix in a more open conformation. The different conformations observed in both bound and apo states indicate a flexible and adaptable active site, which explains how LspA accommodates and processes such a variety of substrates.

Statement of Significance

The functional conformational dynamics of the membrane enzyme lipoprotein signal peptidase (LspA) are on the ns timescale and facilitate an equilibrium of states hypothesized to be important for antibiotic and substrate binding as well as enzymatic activity. The apo protein fluctuates between an open conformation required for substrate binding and a closed state which occludes active site residues from the hydrophobic membrane. The antibiotic globomycin stabilizes an intermediate conformation that inhibits signal peptide cleavage and substrate binding. A hybrid experimental design using MD and EPR facilitated identification of protein conformations not observed previously in crystal structures, and will aid future development of therapeutics.

Main Text

Introduction

With the rapid growth of antibiotic resistance, new drugs that target novel bacterial pathways such as the lipoprotein processing pathway need to be developed. The enzymes involved (Figure S1) in lipoprotein processing are found universally across the bacterial phylogenetic tree, are essential in many organisms including *E. coli*, *S. enterica*, and *M. tuberculosis*, and have no mammalian homologs (1, 2). Lipoproteins are characterized by an N-terminal lipid moiety that serves as a membrane anchor, and perform a wide range of functions including signal transduction, stress sensing, virulence, cell division, nutrient uptake, adhesion, and triggering the activation of host innate immune responses (3, 4). If lipoproteins are processed incorrectly these vital functions and the bacteria are compromised. Lipoprotein signal peptidase (LspA) is an aspartyl protease that performs the second step in the lipoprotein processing pathway - cleaving the transmembrane helix signal peptide of lipoproteins, after lipidation by phosphatidylglycerol-prolipoprotein diacylglyceryl transferase (Lgt) (Figure S1).

Structures of LspA from *P. aeruginosa* (LspPae) and *S. aureus* (LspMrs) were determined with the antibiotic globomycin bound, and LspMrs was also captured with the antibiotic myxovirescin bound (2, 5). Neither of these antibiotics are commercially viable, but provide hypotheses of substrate interactions, conformational changes, and the catalytic cycle. The catalytic dyad residues (Figure S2) and 14 additional highly conserved residues that surround the active site were identified. The extensive conservation indicates that resistance mutations arising within the active site to impede antibiotic binding would also likely interfere with the binding and cleavage of substrate (2). Thus, LspA is a powerful target to combat the development of antibiotic resistance.

The apo and lipoprotein bound structures of LspA have not been determined and, thus, an understanding of the conformational dynamics associated with substrate binding and signal peptide cleavage is not fully understood. Based on lipid (from crystallization conditions) and globomycin interactions in the crystal structure, the orientation of lipoprotein substrate bound to LspA was proposed in which the β-cradle and highly conserved periplasmic helix (PH) “clamp” the substrate in place (2, 5). A comparison of the LspA conformations with the two different antibiotics bound indicated that the PH can adopt different

conformations and the antibiotic can adopt different orientations (Figure S2) while maintaining similar interactions with the catalytic diad (5). Based on this model, we hypothesize that the β-cradle and PH must undergo conformational dynamics in order to allow the different lipoprotein substrates to enter into the active site. We investigated the "clamp" hypothesis using molecular dynamics (MD) simulations and electron paramagnetic resonance (EPR) studies. This hybrid approach determined that the "clamp" in the apo state is solely the result of PH fluctuations on the nanosecond time scale with the dominant conformation of the PH over the active site to occlude the polar catalytic diad from the lipid bilayer and a minor conformation that partially exposes the active site. These states were visualized by selecting structures from the molecular dynamics trajectories that agreed with experimental EPR restraints.

Materials and Methods

Molecular dynamics simulation setup. All simulations were run using GROMACS 2018 (6). The Martini 2.2 force field (7) was used to run an initial 200 ns Coarse Grained (CG) MD simulation to permit the assembly and equilibration of a palmitoyloleolylphosphatidylglycerol (POPG) palmitoyloleoylphosphatidylethanolamine (POPE) (1:4 mole ratio) bilayer around LspA (PDB: 5DIR) (2). An elastic network of 1000 kJ mol^{-1} nm^{-2} was applied between all backbone beads between 0.5 and 1 nm. Electrostatics were described using the reaction field method, with a cut-off of 1.1 nm using the potential shift modifier and the van der Waals interactions were shifted between 0.9-1.1 nm. The systems were first energy minimized by steepest descent algorithm to 1000 kJ mol^{-1} nm^{-1} and then simulated for a total of 200 ns. The temperature and pressure were kept constant throughout the simulation at 310 K and 1 bar respectively, with protein, lipids, and water/ions coupled individually to a temperature bath by the V-rescale method (8) and a semi-isotropic Parrinello-Rahman barostat (9). The final snapshots from the CG simulations were then converted back to an atomistic description using CG2AT (10).

Atomistic simulations. The truncated charged C- termini of the converted protein was capped using a methyl moiety. All ionisable groups were simulated with default protonation states, unless otherwise mentioned. The virtual site model for hydrogen atoms (11), adapted for the CHARMM36 forcefield (12) was employed, allowing the use of a 4 fs timestep during the simulations. Electrostatics were described using PME, with a cut-off of 1.2 nm and the van der Waals interactions were shifted between 1-1.2 nm. The tip3p water model was used, and the water bond angles and distances were constrained by SETTLE (13). All other bonds were constrained using the LINCS algorithm (14). The systems were then equilibrated for a further 1 ns using a 4 fs timestep with positional restraints of 1000 kJ mol^{-1} nm^{-2} on the heavy atoms, in a NPT ensemble with temperature V-rescale coupling at 310 K with protein, lipids (POPG and POPE at a 1:4 molar ratio), and water/ions coupled individually (8) and semi-isotropic Parrinello-Rahman barostat at 1 bar (9). The parameters for globomycin generated using the CHARMM-GUI webserver (15). The apo and globomycin bound production simulations were performed without position restraints for a total of 500 ns, and run in triplicate.

Expression, purification, and spin labeling of LspA. The *Pseudomonas aeruginosa* (strain PAO1) LspA gene was purchased in a pET28b vector with an N-terminal 6xHis tag and thrombin cleavage sequence (General Biosystems Inc., Durham, NC). Cysteine residues were introduced via PIPE Mutagenesis (16) or QuikChange (17) (Agilent, Santa Clara, CA), and gene sequencing confirmed the correct mutations (Genewiz Inc., South Plainfield, NJ). LspA was expressed and purified using a modified previously published protocol (2) (see supplemental materials).

Continuous-wave EPR. CW EPR experiments on singly labeled LspA proteins in FC12 detergent micelles were performed on a CW X-Band EMX spectrometer (Bruker Biospin) at room temperature. The samples were loaded into 0.6 mm glass capillary tubes (VitroCom, Mountain Lakes, NJ) with a sample volume around 7 µL. Spectra were processed with Bruker software (WinEPR), and normalized and analyzed with LabView programs (Base2 and ADJ) provided by Christian Altenbach and Wayne Hubbell (UCLA). For globomycin studies, globomycin (Sigma-Aldrich, St. Louis, MO) was resuspended in DMSO at a concentration of 10 mg/mL. The appropriate amount was aliquoted into tubes and dried in a lyophilizer. The dried globomycin was resuspended with spin labeled LspA sample for EPR studies. This procedure was required because DMSO was shown to have a large impact on CW spectra (Figure S3).

Pulsed EPR. Double-labeled LspA proteins in FC12 detergent micelles were measured using pulsed EPR with a Q-band Bruker ELEXSYS E580 Spectrometer at Q-band and 80 K. All samples were prepared to a final protein concentration around 300 μM with 20% deuterated glycerol with a sample volume of 15 μL. Globomycin samples contained a 20:1 molar ratio of globomycin. The samples were loaded into quartz capillaries with a 1.6 mm od x 1.1 mm id x 100 mm length (VitroCom, Mountain Lakes, NJ) and flash frozen in liquid nitrogen. A four pulse DEER sequence was used with 16-step phase cycling (20 ns π/2 and two 40 ns π observed pulses, and a π pump pulse) (18). The pump frequency was set at the maximum of the nitroxide spectrum and the observed frequency was set to 75 MHz lower. Increasing inter-pulse delays at 16 ns increments were used with a 16-step phase cycle during data collection. Accumulation times were typically between 18 and 24 hours, with a dipolar evolution time around 4 μs. Dipolar evolution data were processed using DEERAnalysis2018 software using two-step Tikhonov regularization to generate the distance distributions (19, 20) shown in the main text and Comparative Data Analysis v2.0 (provided by Gunnar Jeschke) to provide a comparison to using DEERnet or one-step Tikhonov regularization (21, 22). Predicted DEER distributions for crystal structures or MD-derived structures were generated using MMM (23), and simulated DEER distributions from the MD simulation were generated using DEER-PREdict (24).

Results

To determine conformational changes between the apo and globomycin bound states, MD simulations were performed on LspPae in a lipid bilayer (see methods). Excluding termini residues, the highest root mean square fluctuation (RMSF) observed in the MD simulations is in residues of the PH, with the apo state showing larger fluctuation of the PH than the globomycin bound state (Figure S4). Apo LspPae simulations indicate shorter distances sampled between the PH and β-cradle compared to the globomycin bound state; however, both the apo and globomycin bound states sample up to the same maximum distances (Figure 1).

To experimentally investigate the observed conformational dynamics in the MD simulations, LspPae was spin labeled at sites in the PH (A57R1 and A63R1) and β-cradle (V41R1 and I43R1) (Figure S5). Continuous wave (CW) EPR spectra indicate that each of these sites in apo LspPae are in regions with backbone fluctuations in the nanosecond timescale. As expected from the globomycin bound crystal structure and MD simulations, the CW spectra are broadened (indicating decreased mobility of the spin label) upon addition of globomycin for sites in the PH, but not in the β-cradle (Figure S5), and broadening was most dramatic for site A63R1 (Figure 2). Thus, these data suggest that the PH becomes less dynamic when LspPae is bound to globomycin. Furthermore, an additional spectral component appears at higher concentrations of globomycin (Figure 2), indicating a second more immobile conformation of the spin label. The two spin label conformations suggest that there are two binding modes of globomycin, one in which A63R1 remains mobile (but less mobile than the apo state), and another in which A63R1 is more rigid. Interestingly, a comparison of the two LspMrs crystal structures shows that while the two antibiotics maintain interactions with the same catalytic residues, they are oriented differently in the active site (5). Myxovirescin binds more towards the β-cradle side of the active site, allowing the PH to fold over the active site and thus have more tertiary contacts. The analogous residue to LspPae A63 is LspMrs S61, which directly interacts with N53 in the myxovirescin structure and is solvent exposed in the globomycin bound structure (Figure S6). It is possible that globomycin can sample both of these binding sites, with the second component population arising from the second weaker binding site (seen at higher concentrations of globomycin). If the two spin label conformations arise from one globomycin binding site, then the two populations would be influenced equally across the concentrations investigated and saturation should be reached based on the reported IC_{50} (25–28). Flexibility of the active site is consistent with the diverse set of substrate sequences that interact with LspA. The multiple binding modes observed for the antibiotics indicates multiple binding modes are possible for the substrates.

To further investigate LspA conformations observed in solution, double electron-electron resonance (DEER) EPR was used to measure the distance between PH and the β-cradle. One site on the PH and one site on the β-cradle were selected. On the β-cradle, a site with reduced backbone dynamics at the end of a β-strand would provide more information about the conformational dynamics between the two domains than a loop site. The flexibility of the loop site would broaden the distance distribution and complicate the interpretation of changes in distance distributions between states. However, labeling within the strand may

perturb folding. Based on these criteria, residues I43, F47, and W130 were candidates for labeling of the β-cradle because they are not at tertiary contacts. Based on the structure, F47 and W130 would be in position to interact with the membrane headgroups and modulate the stability and dynamics of the β-cradle. In addition, of the three residues, I43 is the furthest away from the PH and is in the optimal distance range for DEER measurements. The PH contains residues 59 through 63. Residue F59 was excluded from consideration as it is highly conserved and has an evolutionary coupling (29–31) to F136 indicating a potential important interaction. The predicted DEER distance distribution between I43 and residue S60, F61, or L62 contained distances at the lower end of DEER detection as modeled with spin labels added to the apo MD structure (Figure S7A) (23). Thus, I43 and A63 were ultimately chosen as the pair that would provide the most information on the conformational changes between the PH and β-cradle. As the distance between only the PH and β-cradle was sought, and all other parts of the protein remained relatively stationary throughout the MD trajectories, additional spin label pairs were not required. Additionally, the distances observed in the MD trajectories between I43 and S60 through A63 followed a similar pattern in both the MD and globomycin simulations (Figure S7B). Therefore, additional spin label pairs for DEER analysis would not give any additional information and were not pursued.

In the apo state, the distance between I43R1 and A63R1 is broad and centered around 2.8 nm. Upon addition of globomycin, these shorter distances are sampled but there is a more populated conformation at 4.5 nm (Figure 3). Analysis of the distance distributions are consistent between two-step or one-step Tikhonov regularization and DEERnet,, which improved the uncertainties associated with each population (Figure S8) (21, 22). These data demonstrate that the β-cradle and PH are closer together in the apo state and can sample two conformations in the saturated globomycin-bound state, agreeing with the two-component CW spectra. In order to directly compare the DEER data to the published crystal structures, spin labels were modeled at the appropriate sites and a predicted DEER distribution was generated (23) for all sterically possible rotamers or a subset selected to fit the experimental DEER data (Figure S9 and S10). Interestingly, the apo DEER distribution and the shorter distances of the globomycin DEER distribution agree well with predicted distributions for the myxovirescin bound LspMrs structure, while the more populated, longer distance in the globomycin DEER distribution agrees with the predicted distributions for both globomycin bound LspA crystal structures (Figure S9).

To directly compare the MD and DEER data, DEER-PREdict was used to generate I43-A63 distance distributions from the MD trajectories (Figure 4A) (24). In both the apo and glomobycin bound states, a population of LspA conformations sampled longer distances in the MD simulations than was observed in the DEER distributions. This was particularly observed in the apo state where the majority of MD conformations were longer than in DEER, while in the globomycin bound state a significant percentage overlapped with the longest DEER peak centered at 4.5 nm (Figure 4A). These results are unsurprising considering there is no biasing of the rotamer weighting to fit the data and that averaging over all the states in the MD simulation isn't likely to represent the population probabilities of all the experimentally observed states. To gain more insight into the specific conformational states observed in the MD simulations, spin labels were modeled onto protein databank (PDB) snapshots corresponding to distances of interest from the simulations (arrows in Figure 1) and a predicted DEER distribution was generated (23) (Figure 4B-D). A structure corresponding to the shorter I43-A63 distance peak at 3.2 nm from the apo LspPae simulations correlated to some of the distances observed in the experimental DEER distribution for apo LspPae (Figure 4B), but longer distances were also present that were not observed in the DEER distributions. An MD-derived structure corresponding to the most populated distance (3.8 nm) in the globomycin bound simulation agrees well with the longer, most populated peak of the globomycin DEER distribution (Figure 4C). The rotamer optimized fit to the experimental data is slightly broadened artificially due to the attempt to fit all distance populations rather than only the longer distance (Figure S10). Longer distances are also observed in both the apo and globomycin MD simulations between 3.8 and 4.5 nm (Figure 1). A third structure, which represents a distance of 4.1 nm in the middle of this range, generates distances longer than the observed distances in either the apo or globomycin bound experimental DEER distributions (Figure 4D).

Discussion

Using crystal structures, MD simulations, and CW and DEER EPR, the plasticity of antibiotic binding and the conformation states of LspA are identified, providing a better understanding of how therapeutics could inhibit this essential bacterial enzyme. Each approach in isolation has its limitations, and only in combination we were able to visualize and map the conformational dynamics. The only conformational change observed is the repositioning of the PH, which occurs in the nanosecond time regime as assessed with CW EPR and MD simulations (Figure 5 and S11). In the most closed MD-derived structure, which agrees with the apo DEER distribution and shorter distances of the globomycin DEER distribution, the β-cradle and PH are only 6.2 Å apart, completely occluding the charged and polar active site residues (Figure 5). The structure with an intermediate PH to β-cradle distance agrees with the most populated globomycin bound DEER peak and may also represent the clamped substrate bound state. The most open conformation, as seen only in the MD simulations, has a trigonal cavity where the lipoprotein, signal peptide, and DAG moiety of the lipoprotein substrate are hypothesized to bind, and is the only structure where lipoprotein substrate could sterically fit in the active site (Figure S12). Thus, the open conformation of LspA is the only conformation of the three that would allow the prolipoprotein to enter into and bind in the active site of LspA in the correct orientation for signal peptide cleavage. Although this distance is not observed in the experimental DEER data, the population may be too small to detect and/or not stabilized in the membrane mimic chosen. The two-component CW line shape (Figure 2), multiple distance populations observed for globomycin bound LspA (Figures 1, 3, and 4), and analysis of the crystal structures (Figure S6 and S9) suggest that LspA samples all three of these conformations (closed, intermediate, and open) in all states (apo, globomycin bound, and myxovirescin bound), but the populations of each of these conformations varies in each state. Combining the different conformations observed in the crystal structures, MD simulations, and CW and DEER experimental data, the conformational states required for LspA to cleave the signal peptide from essential lipoproteins were elucidated.

Author Contributions

All authors designed research and wrote the paper; T.C. performed EPR experiments; O.V. performed MD simulations, J.C. performed DEER-PREdict analysis.

Declaration of Interest

The authors declare no competing interests.

Acknowledgments

This work was funded by the National Institutes of Health under grant R35 GM13182 (L.C) and Biophysical Training Grant (5T32GM080186–07 T.A.C.) and the National Science Foundation under grant MCB1817735 (LC). P.J.S's lab is supported by Wellcome [208361/Z/17/Z], BBSRC [BB/P01948X/1, BB/R002517/1 and BB/S003339/1] and MRC [MR/S009213/1]. ARCHER UK National Supercomputing Service (http://www.archer.ac.uk), provided by HECBioSim, the UK High End Computing Consortium for Biomolecular Simulation (hecbiosim.ac.uk), which is supported by the EPSRC (EP/L000253/1). We acknowledge the use of Athena at HPC Midlands+, which was funded by the EPSRC on grant EP/P020232/1, and the University of Warwick Scientific Computing Research Technology Platform for computational access.

References

1. Buddelmeijer, N. 2015. The molecular mechanism of bacterial lipoprotein modification-How, when and why? *FEMS Microbiol. Rev.* 39:246–261.

2. Vogeley, L., T. El Arnaout, J. Bailey, P.J. Stansfeld, C. Boland, and M. Caffrey. 2016. Structural basis of lipoprotein signal peptidase II action and inhibition by the antibiotic globomycin. *Science (80-.).* 351:876–880.

3. Nakayama, H., K. Kurokawa, and B.L. Lee. 2012. Lipoproteins in bacteria: Structures and biosynthetic pathways. *FEBS J.* 279:4247–4268.

4. Szewczyk, J., and J.F. Collet. 2016. The Journey of Lipoproteins Through the Cell: One Birthplace, Multiple Destinations. 1st ed. Elsevier Ltd.

5. Olatunji, S., X. Yu, J. Bailey, C. Huang, M. Zapotoczna, K. Bowen, M. Rem, R. Müller, E.M. Scanlan, J.A. Geoghegan, V. Olieric, and M. Caffrey. 2020. Structures of lipoprotein signal peptidase II from Staphylococcus aureus complexed with antibiotics globomycin and myxovirescin. *Nat. Commun.* 11.

6. Abraham, M.J., T. Murtola, R. Schulz, S. Páll, J.C. Smith, B. Hess, and E. Lindah. 2015. Gromacs: High performance molecular simulations through multi-level parallelism from laptops to supercomputers. *SoftwareX*. 1–2:19–25.

7. de Jong, D.H., G. Singh, W.F.D. Bennett, C. Arnarez, T.A. Wassenaar, L. V. Schäfer, X. Periole, D.P. Tieleman, and S.J. Marrink. 2013. Improved parameters for the martini coarse-grained protein force field. *J. Chem. Theory Comput.* 9:687–697.

8. Bussi, G., D. Donadio, and M. Parrinello. 2007. Canonical sampling through velocity rescaling. *J. Chem. Phys.* 126.

9. Parrinello, M., and A. Rahman. 1981. Polymorphic transitions in single crystals: A new molecular dynamics method. *J. Appl. Phys.* 52:7182–7190.

10. Stansfeld, P.J., and M.S.P. Sansom. 2011. From coarse grained to atomistic: A serial multiscale approach to membrane protein simulations. *J. Chem. Theory Comput.* 7:1157–1166.

11. Feenstra, K.A., B. Hess, and H.J.C. Berendsen. 1999. Improving efficiency of large time-scale molecular dynamics simulations of hydrogen-rich systems. *J. Comput. Chem.* 20:786–798.

12. Olesen, K., N. Awasthi, D.S. Bruhn, W. Pezeshkian, and H. Khandelia. 2018. Faster Simulations with a 5 fs Time Step for Lipids in the CHARMM Force Field. *J. Chem. Theory Comput.* 14:3342–3350.

13. Miyamoto, S., and P.A. Kollman. 1992. Settle: An analytical version of the SHAKE and RATTLE algorithm for rigid water models. *J. Comput. Chem.* 13:952–962.

14. Hess, B., H. Bekker, H.J.C. Berendsen, and J.G.E.M. Fraaije. 1997. LINCS: A linear constraint solver for molecular simulations. *J. Comput. Chem.* 18:1463–1472.

15. Jo, S., T. Kim, V.G. Iyer, and W. Im. 2008. CHARMM-GUI: A web-based graphical user interface for CHARMM. *J. Comput. Chem.* 29:1859–1865.

16. Klock, H.E., and S.A. Lesley. 2009. The Polymerase Incomplete Primer Extension (PIPE) Method Applied to High-Throughput Cloning and Site-Directed Mutagenesis Heath. In: Methods in Molecular Biology: High Throughput Proetin Expression and Purification. . pp. 91–103.

17. Xia, Y., and L. Xun. 2017. Revised Mechanism and Improved Efficiency of the QuikChange Site-Directed Mutagenesis Method. In: Reeves A, editor. In Vitro Mutagenesis: Methods and Protocols. New York, NY: Springer New York. pp. 367–374.

18. Pannier, M., S. Veit, A. Godt, G. Jeschke, and H.W. Spiess. 2000. Dead-Time Free Measurement of Dipole-Dipole Interactions between Electron Spins. *J. Magn. Reson.* 142:331–340.

19. Jeschke, G., V. Chechik, P. Ionita, A. Godt, H. Zimmermann, J.E. Banham, C.R. Timmel, D. Hilger, and H. Jung. 2006. DeerAnalyis 2006- a Comprehensive Software Package for Analyzing Pulsed ELDOR Data. *Appl. Magn. Reson.* 30:473–498.

20. Jeschke, G. 2012. DEER Distance Measurements on Proteins. *Annu. Rev. Phys. Chem.* 63:419–46.

21. Schiemann, O., C.A. Heubach, D. Abdullin, K. Ackermann, M. Azarkh, E.G. Bagryanskaya, M. Drescher, B. Endeward, J.H. Freed, L. Galazzo, D. Goldfarb, T. Hett, L. Esteban Hofer, L. Fábregas Ibáñez, E.J. Hustedt, S. Kucher, I. Kuprov, J.E. Lovett, A. Meyer, S. Ruthstein, S. Saxena, S. Stoll, C.R. Timmel, M. Di Valentin, H.S. McHaourab, T.F. Prisner, B.E. Bode, E. Bordignon, M. Bennati, and G. Jeschke. 2021. Benchmark Test and Guidelines for DEER/PELDOR Experiments on Nitroxide-Labeled Biomolecules. *J. Am. Chem. Soc.* 143:17875–17890.

22. Worswick, S.G., J.A. Spencer, G. Jeschke, and I. Kuprov. 2018. Deep neural network processing of DEER data. *Sci. Adv.* 4.

23. Jeschke, G. 2018. MMM: A toolbox for integrative structure modeling. *Protein Sci.* 27:76–85.

24. Tesei, G., J.M. Martins, M.B.A. Kunze, Y. Wang, R. Crehuet, and K. Lindorff-Larsen. 2021. DEER-PREdict: Software for efficient calculation of spin-labeling EPR and NMR data from conformational ensembles. *PLoS Comput. Biol.* 17:1–18.

25. Dev, I.K., and P.H. Ray. 1984. Rapid assay and purification of a unique signal peptidase that processes the prolipoprotein from Escherichia coli B. *J. Biol. Chem.* 259:11114–11120.

26. Tokunaga, M., J.M. Loranger, and H.C. Wu. 1984. Prolipoprotein modification and processing enzymes in Escherichia coli. *J. Biol. Chem.* 259:3825–3830.

27. Kitamura, S., A. Owensby, D. Wall, and D.W. Wolan. 2018. Lipoprotein Signal Peptidase Inhibitors with Antibiotic Properties Identified through Design of a Robust In Vitro HT Platform. *Cell Chem. Biol.*

28. Kitamura, S., and D.W. Wolan. 2018. Probing substrate recognition of bacterial lipoprotein signal peptidase using FRET reporters. *FEBS Lett.*

29. Nicoludis, J.M., and R. Gaudet. 2018. Applications of sequence coevolution in membrane protein biochemistry. *Biochim Biophys Acta*. 1860:895–908.

30. Kamisetty, H., S. Ovchinnikov, and D. Baker. 2013. Assessing the utility of coevolution-based residue-residue contact predictions in a sequence- and structure-rich era. *Proc. Natl. Acad. Sci.* 110:15674–15679.

31. Ovchinnikov, S., H. Kamisetty, and D. Baker. 2014. Robust and accurate prediction of residue-residue interactions across protein interfaces using evolutionary information. *Elife*. 2014:1–21.

Figure Captions

Figure 1. MD results of LspPae conformational states. I43 Cα – A63 Cα distance measured over apo (black) and globomycin bound (red) MD simulations. The I43 Cα – A63 Cα distance of selected structures are labeled.

Figure 2. EPR CW spectra of LspPae PH residue A63R1. Increasing concentrations of globomycin broaden the spectra and show a second structural element (arrow) indicating a second, more rigid conformation. Colors represent mole ratio of globomycin to LspPae as indicated in insert.

Figure 3. Top) Best fit of I43R1/A63R1 DEER echo decay (gray) for apo (black, left) and globomycin bound (red, right) LspPae. Bottom) DEER distributions of I43R1/A63R1 LspPae. The apo distribution (black, left) shows a broad distance distribution while the addition of globomycin (red, right) at a 20:1 molar ratio shows a large population of distances around 4.5 nm. Distribution uncertainty is shown in gray.

Figure 4. MD analysis of LspPae conformational states. A) DEER-PREdict distance distributions from MD trajectories (red) compared to experimental DEER distributions (black) for apo (left) and globomycin bound (right) states. The dark red MD distribution is the average of three individual simulations (pale red lines). Colored arrows in Figure 1 indicate distances of extracted structures used to generate predicted DEER distributions in B (gray), C (maroon), and D (blue). The 3.8 nm (maroon) and 4.1 nm (blue) structures were extracted from the globomycin simulations. However, those distances are observed in both globomycin bound and apo MD simulations. Predicted DEER distributions of spin labeled structures from the MD simulations are shown in solid lines while predicted distributions with the spin label rotamers optimized to fit the experimental DEER distributions (apo, black (B); and globomycin, red (C)) are shown in dashed lines.

Figure 5. LspA protein electrostatics. Charged residues in the active site are hidden in the closed conformation (left) and are increasingly exposed as the PH moves away from the β-cradle in the intermediate (middle) and open (right) conformations. Negatively charged residues are shown in red and positively charged residues in blue.

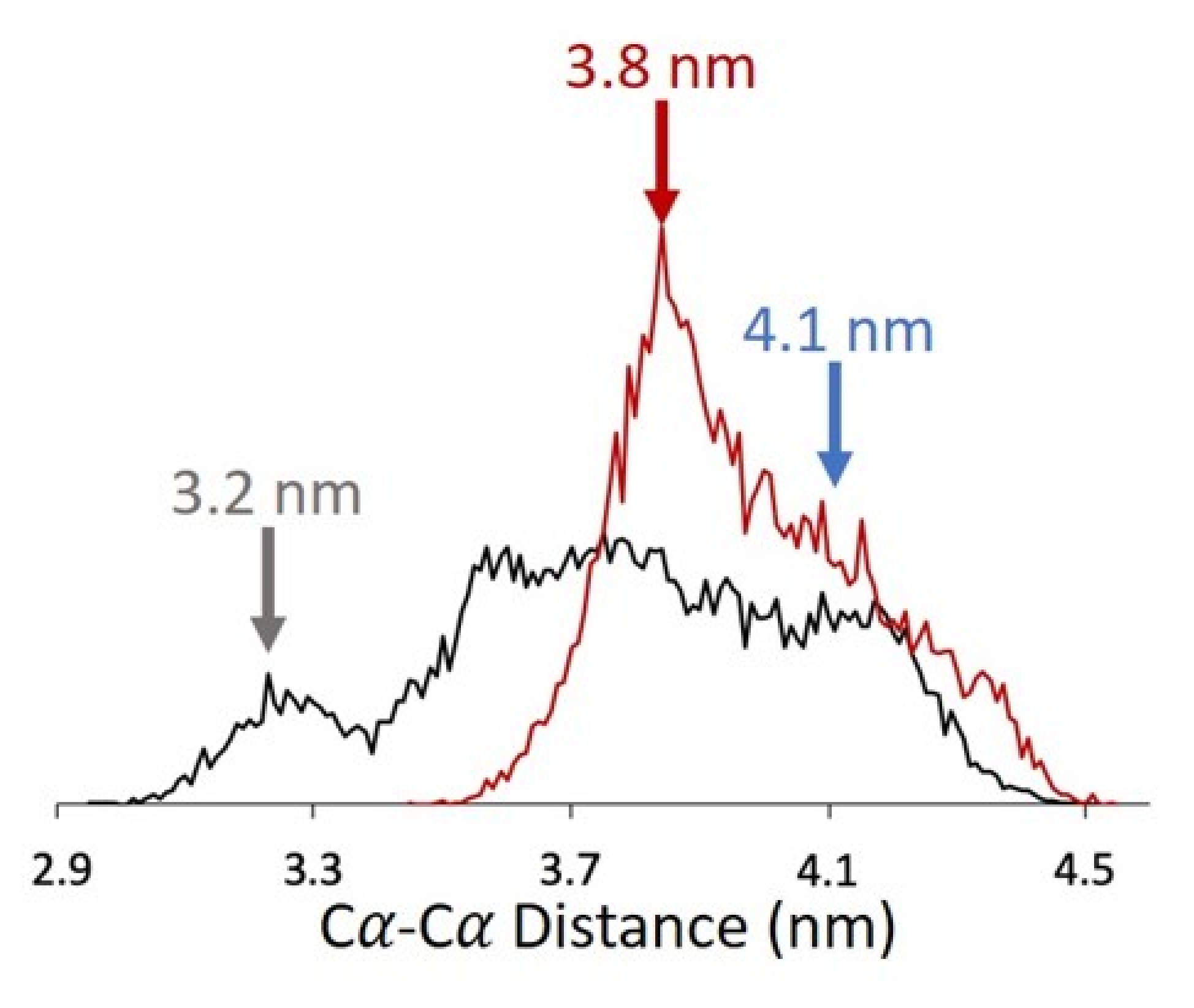
3.8 nm
4.1 nm
3.2 nm
2.9
3.3
3.7
4.1
4.5
Cα-Cα Distance (nm)

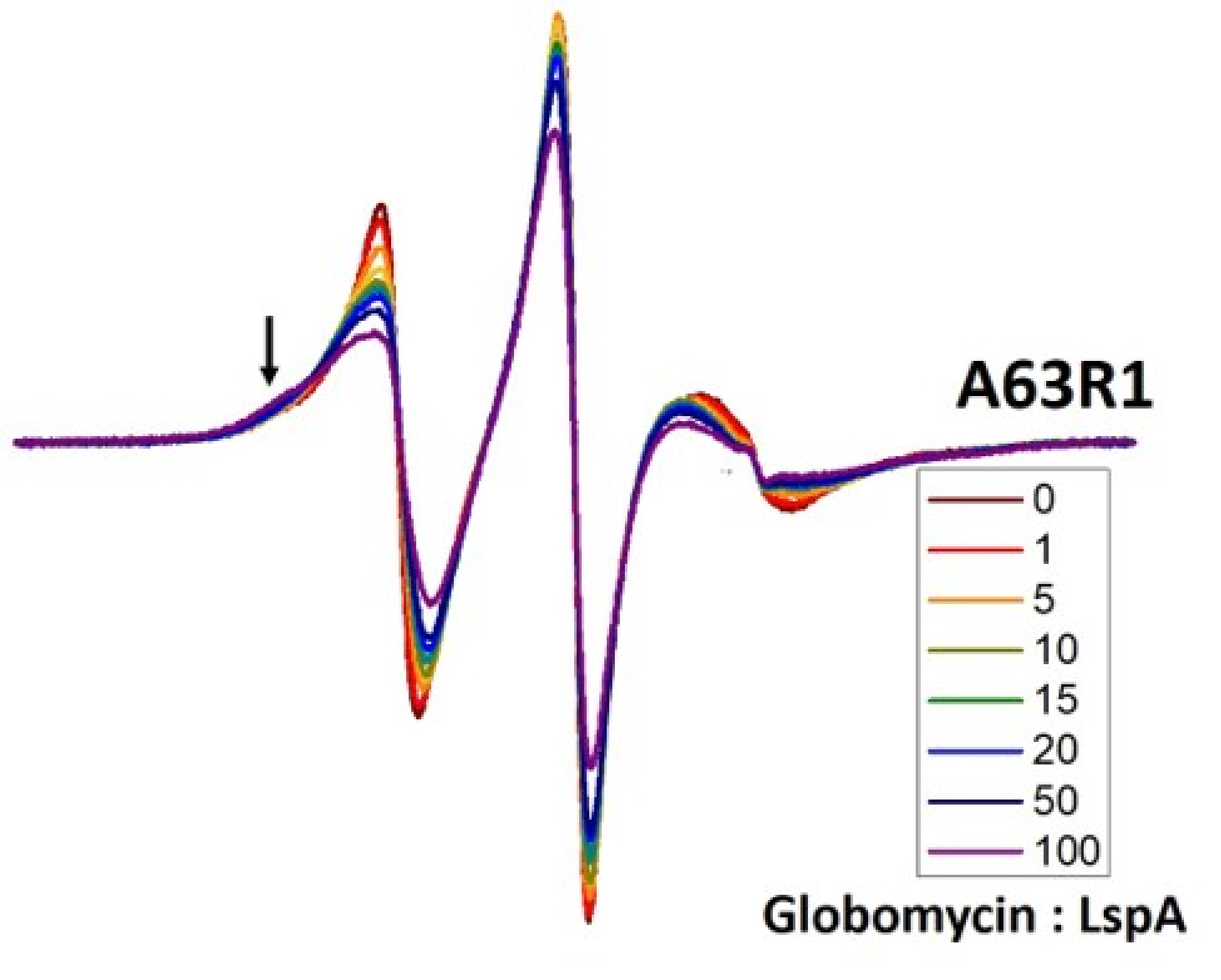
A63R1
0
1
5
10
15
20
50
100
Globomycin : LspA

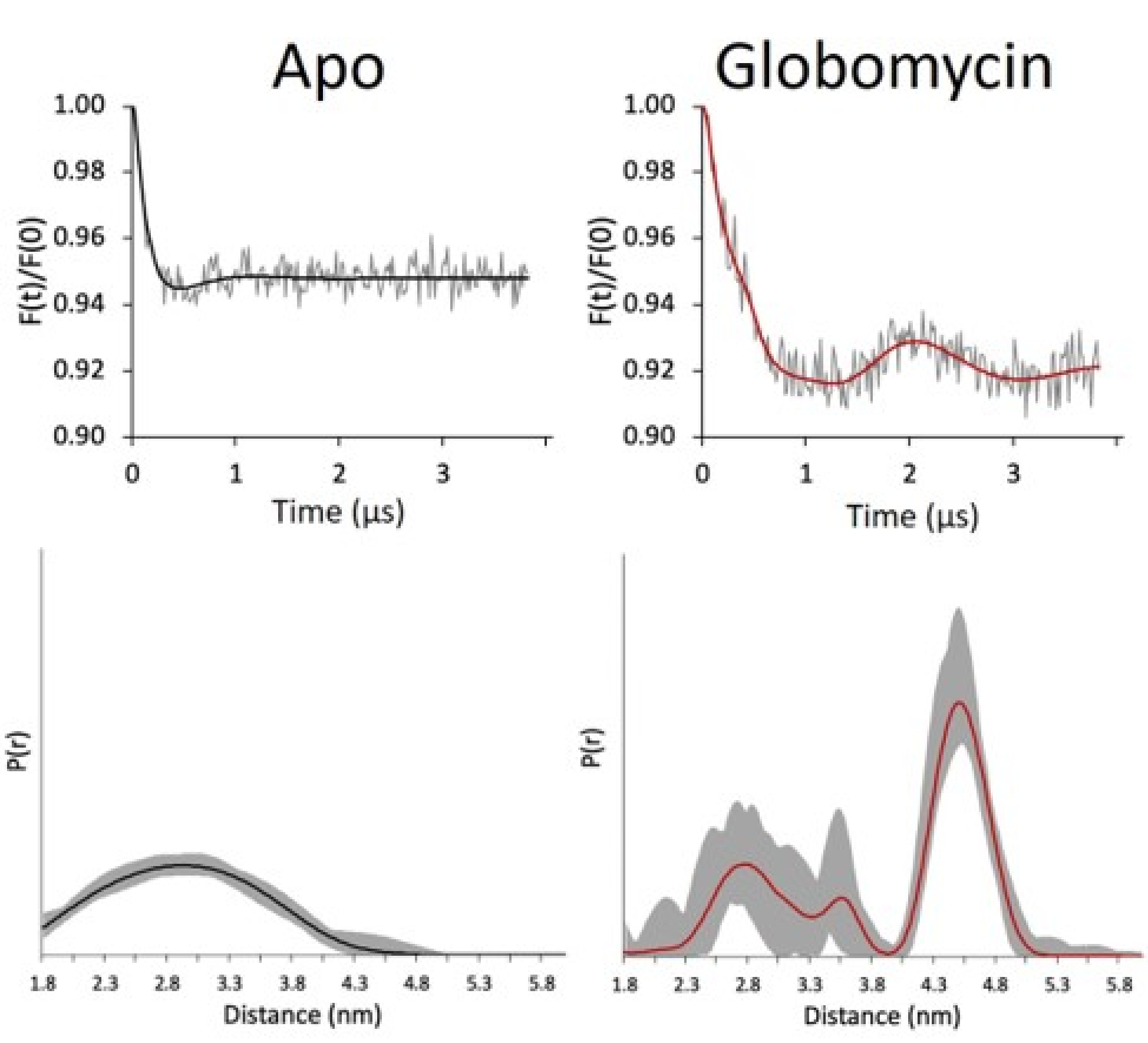
Apo
Globomycin
1.00
0.98
0.96
0.94
0.92
0.90
F(t)/F(0)
0
1
2
3
Time (µs)
P(r)
1.8
2.3
2.8
3.3
3.8
4.3
4.8
5.3
5.8
Distance (nm)

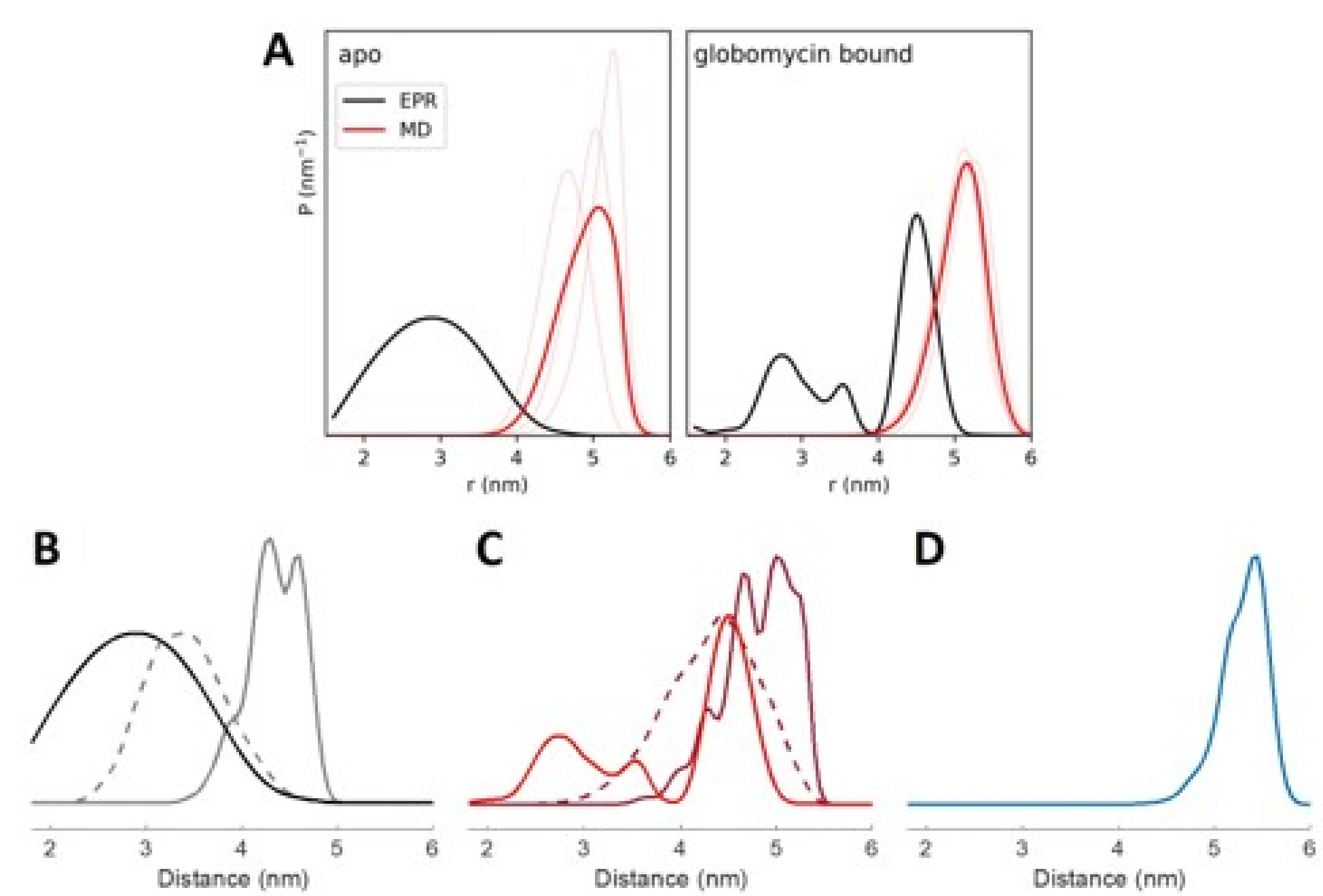
A
apo
globomycin bound
EPR
MD
P (nm⁻¹)
r (nm)
r (nm)
B
C
D
Distance (nm)
Distance (nm)
Distance (nm)

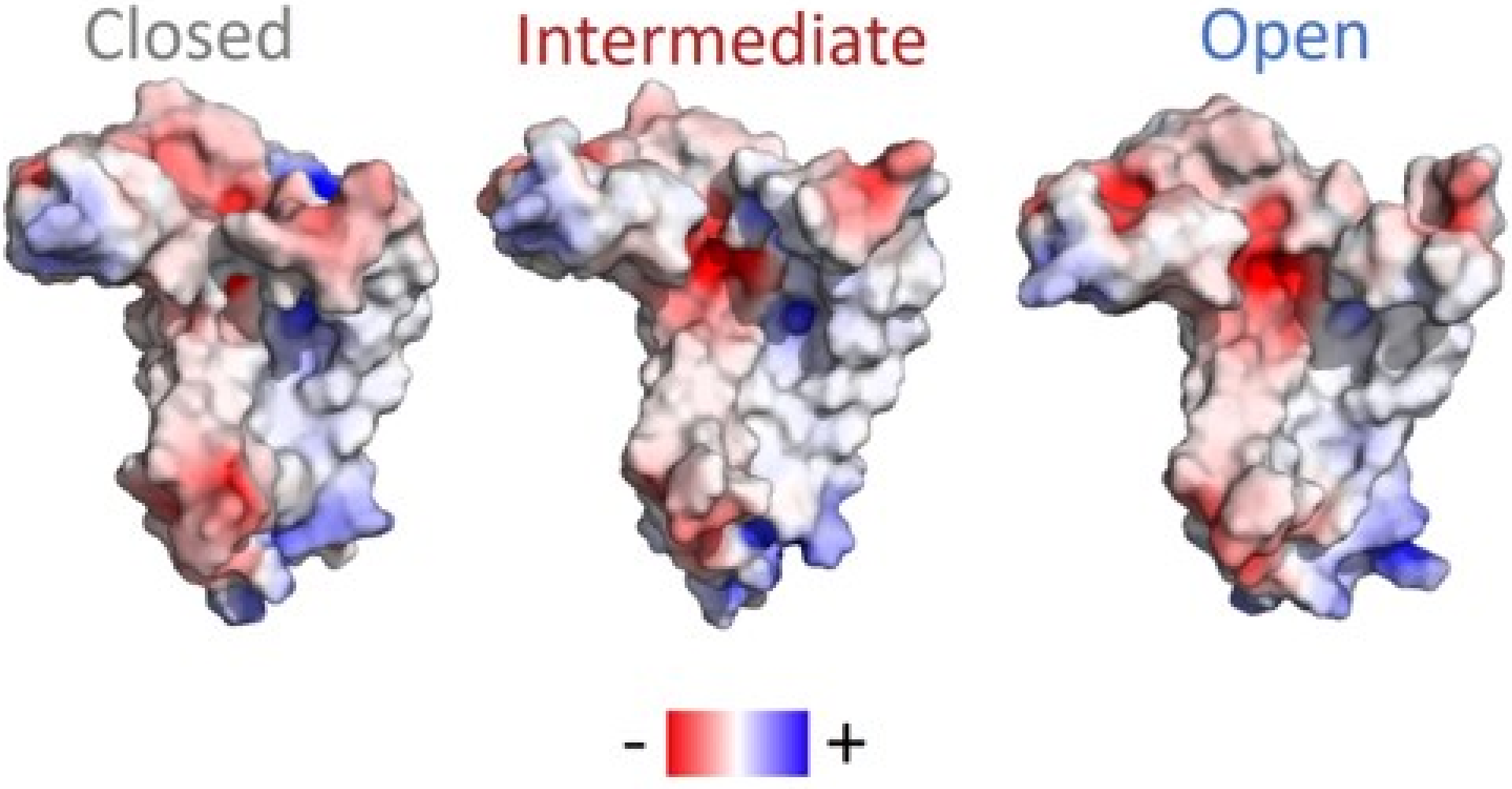
Closed
Intermediate
Open
-
+

Supplemental Information for

Conformational dynamics of the membrane enzyme LspA upon antibiotic and substrate binding

Tracy A. Caldwell, Owen N. Vickery, Johnathan D. Colburn, Phillip J. Stansfeld, Linda Columbus

Extended Methods

Protein Purification. The LspA plasmids were transformed into C41(DE3) *E. coli* cells (Lucigen) and cultures were grown in Luria-Burtani (LB) media supplemented with 50 mg/L kanamycin to an OD600 around 0.8. Expression was induced with 1 mM isopropyl-β-thio-D-galactoside (IPTG) for around 18 hours at 25°C. Cells were harvested by centrifugation at 5,000g for 10 min at 4 °C and the pellets were frozen at -20 °C. Cells were resuspended in Buffer A (20 mM phosphate, pH 7.2, 150 mM NaCl) with one Complete Protease Inhibitor Cocktail tablet (Roche) and passed twice through a high-pressure Nano DeBEE homogenizer (BEE International). Cell debris were removed via centrifugation at 18,000g for 30 min. The membrane fraction was subsequently separated by ultra-centrifugation at 150,000g for 1 hour at 4 °C. The membrane pellet was resuspended in 30 mL Buffer A and frozen at -80 °C. The membrane resuspension was thawed and 10 mL Buffer A containing fos choline-12 (FC12) was added such that the final concentration of FC12 was 1.8% (w/v) and was allowed to rock at 4 °C for at least one hour. Unsolubilized material was then removed by ultracentrifugation at 100,000g for 45 min. Recombinant LspA protein was bound to a Ni^{2+} immobilized metal affinity chromatography column, washed with Buffer A containing 40 mM imidazole and 0.14% (w/v) FC12. For spin labeling, 10 mL Buffer A containing 40 mM imidazole and 0.7 mM MTSL/R1 spin label (S-(2, 2, 5, 5-tetramethyl-2,5- dihydro-1H-pyrrol-3-yl)methyl methanesulfonothioate, Toronto Research Chemicals Inc.) was added and the column was allowed to nutate at 4 °C overnight. The next day, the column was further washed with 20 mL Buffer A with 40 mM imidazole and 0.14% (w/v) FC12 to remove free R1 and spin labeled protein was eluted in 10 mL Buffer A containing 300 mM imidazole and 0.14% (w/v) FC12. Imidazole was removed over a PD-10 column (GE Healthcare Biosciences) and the protein was concentrated to around 300 mM using a 10kDa molecular weight cutoff concentrator (Millipore). Protein purity was assessed by SDS-PAGE and the protein was confirmed as LspA with MALDI-TOF mass spectrometry.

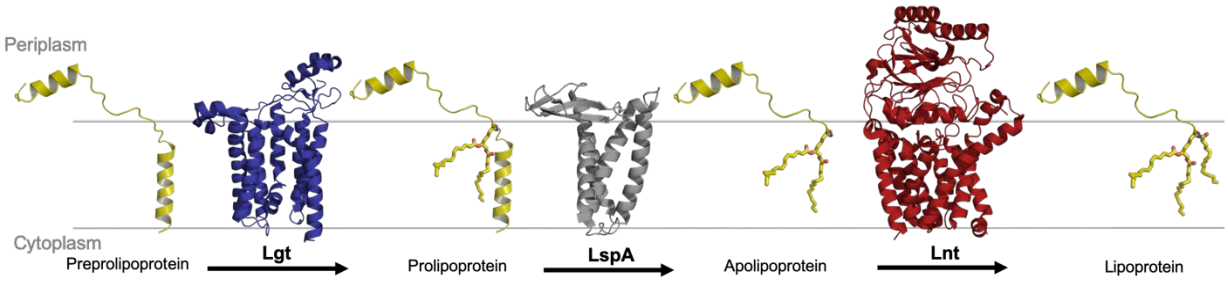

Figure S1. Lipoprotein processing pathway in Gram-negative bacteria. After diacylation of the substrate cysteine (LppL, yellow) by Lgt (blue), LspA (gray) cleaves the signal peptide from the substrate. Lnt (red) then N-acylates the lipid modification of the substrate. Gram-positive bacteria lack Lnt. The membrane is represented by gray lines. PDB IDs for the structures shown: Lgt:5AZC (*E. coli*), LspA: 5DIR (*P. aeruginosa*), Lnt: 5N6H (*E. coli*), LppL (*P. aeruginosa*, was created *in silico*).

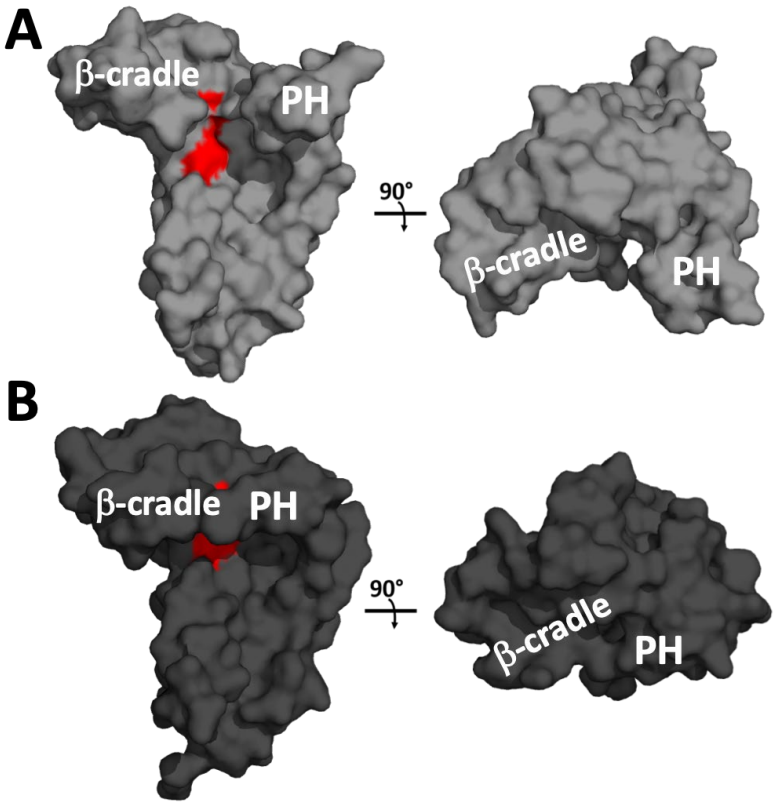

Figure S2. Hypothesized LspA conformational dynamics. The LspPae crystal structure with the antibiotic globomycin bound (A) and LspMrs with the antibiotic myxovirescin bound (B) provide two structures that lead to a hypothesis that conformational dynamics of the PH and β-cradle open (exposing the catalytic dyad, red) to allow native substrates to bind in the active site, and close to occlude the charged residues.

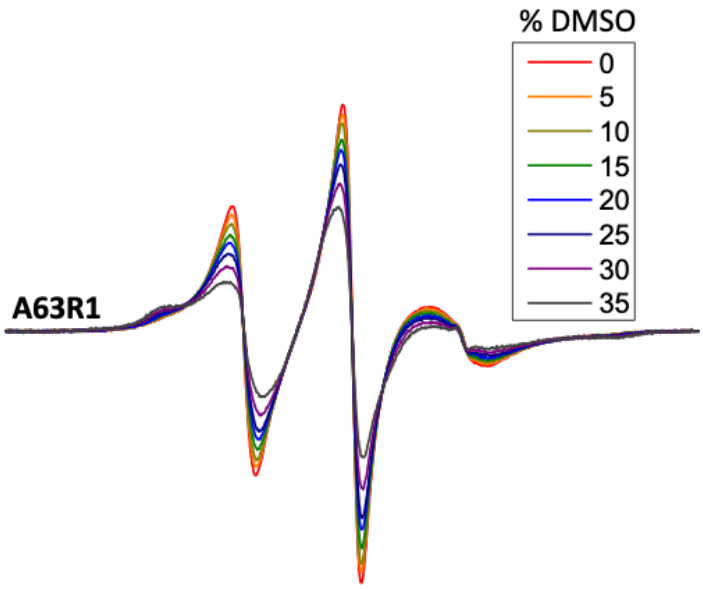

Figure S3. EPR CW spectra of LspA β-cradle residue A63 with increasing amounts of DMSO. DMSO disrupts the spectral line shape indicating a change in structure.

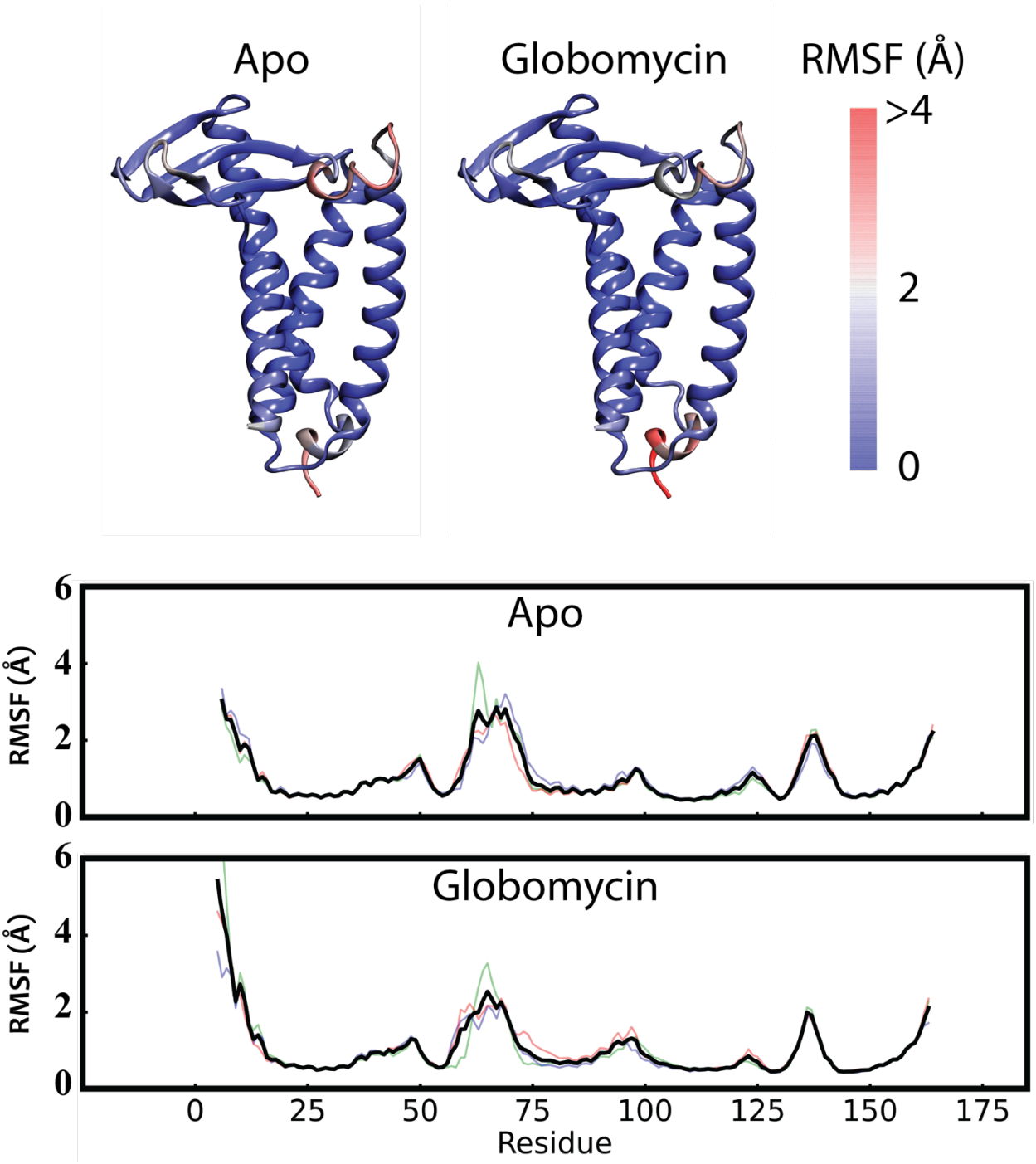

Figure S4. Root mean squared fluctuation (RMSF) observed throughout LspPae apo and globomycin bound MD trajectories shown mapped onto the LspA structure (top) and plotted by residue (bottom) for three MD repeats (green, blue, and red) and the average of the three repeats (black). The PH region (residues 59-63) have the highest fluctuation and the last β-turn in the β-cradle (residues 130-134) has the second highest fluctuation compared to the rest of the protein (excluding the protein termini).

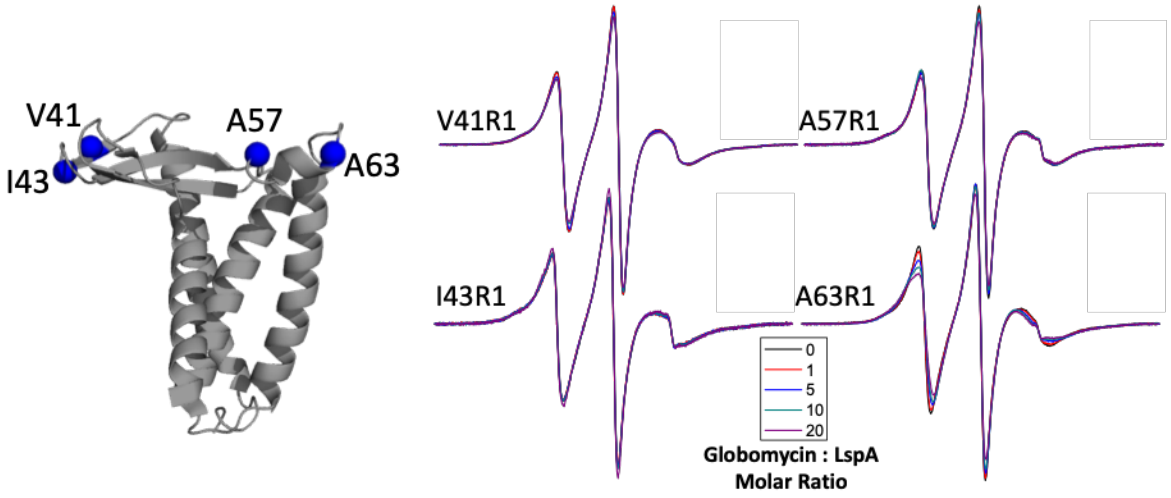

Figure S5. EPR CW spectra (right) for several spin label sites on LspPae (left). The addition of globomycin shows a greater effect on PH residue mobility than on β-cradle residues, with the greatest effect seen at residue A63.

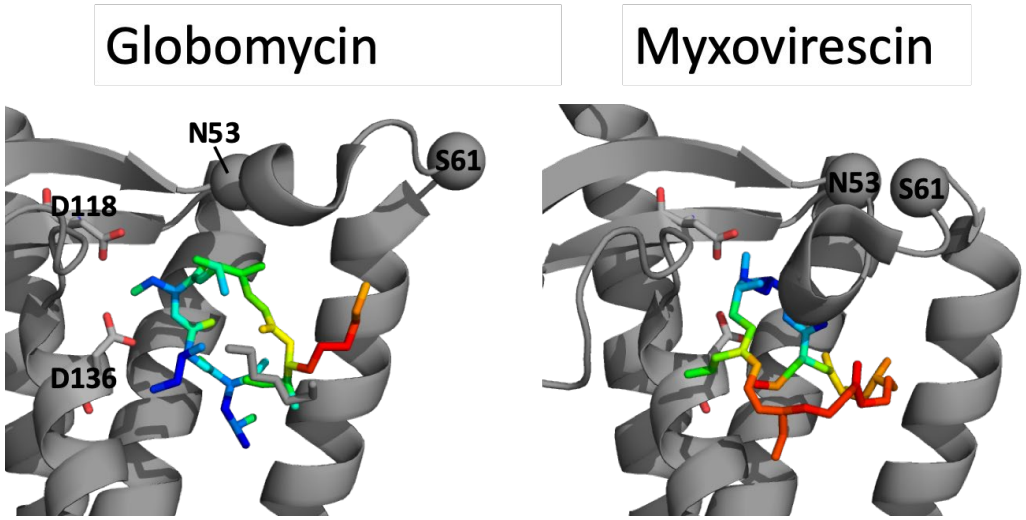

Figure S6. Location of spin label site in LspMrs. S61, the analogous residue to A63 in LspPae, is on a solvent exposed loop in the globomycin bound structure, but has tertiary contacts to N53 in the myxovirescin bound structure. The antibiotics are colored by B-factor from blue (low) to red (high). PDB IDs 6RYO (globomycin bound, left) and 6RYP (myxovirescin bound, right). Catalytic residues D118 and D136 shown as sticks.

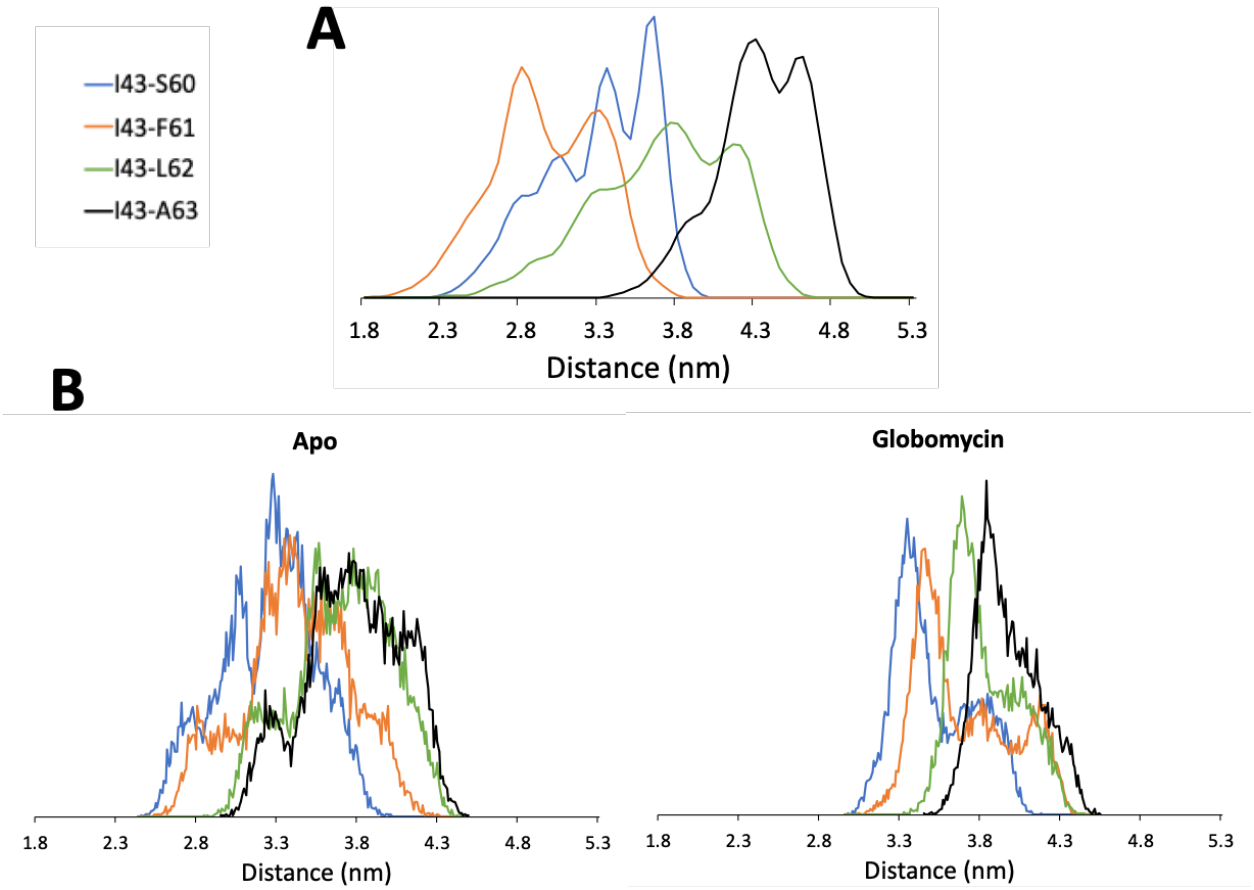

Figure S7. Selection of spin labeled residues for DEER. A) MMM simulation from apo MD structure. B) Pairwise Cα-Cα distances measured throughout the MD apo (left) and globomycin (right) trajectories.

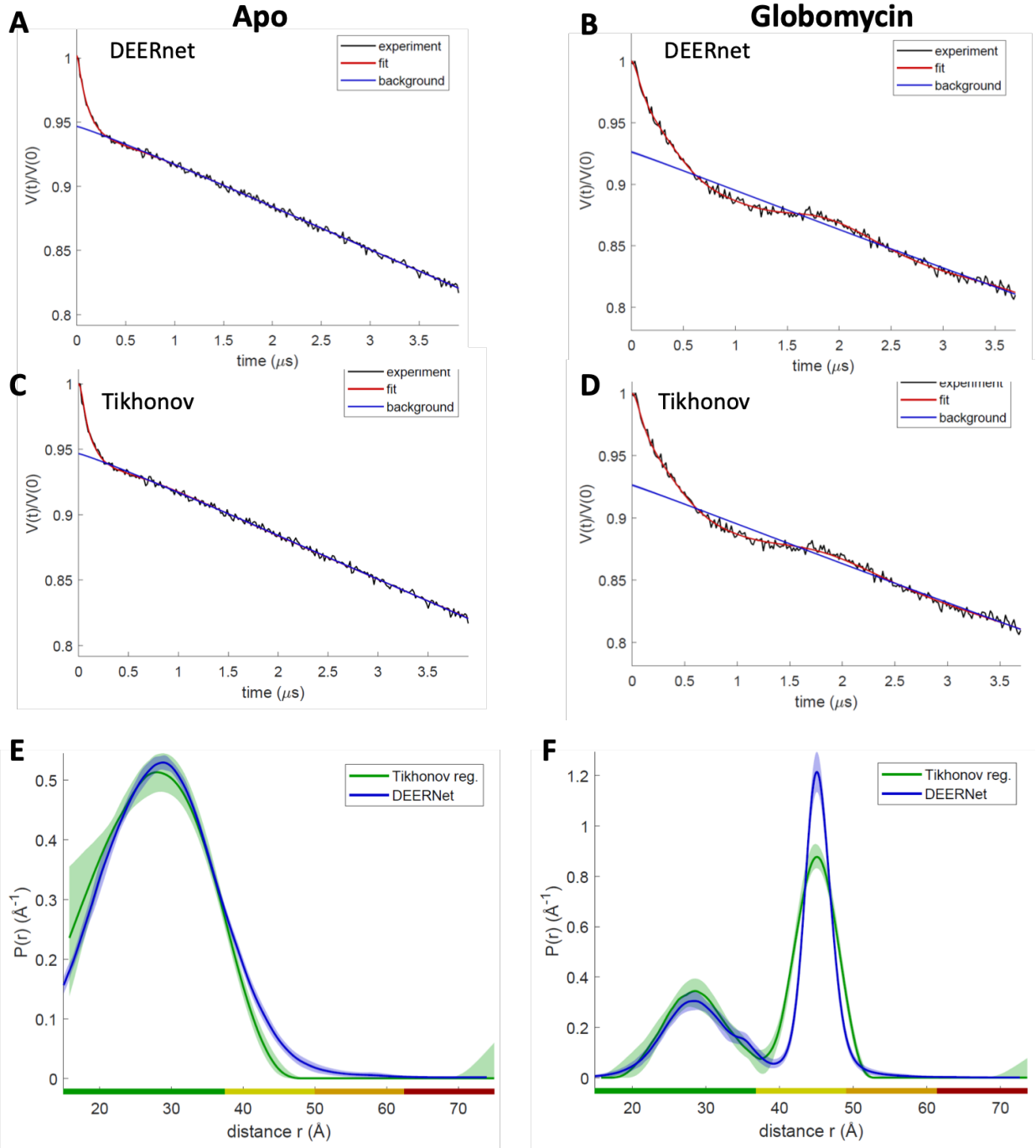

Figure S8. Comparison of one-step Tikhonov and DEERnet approaches to background subtraction (A-D) and distances distributions (E and F).

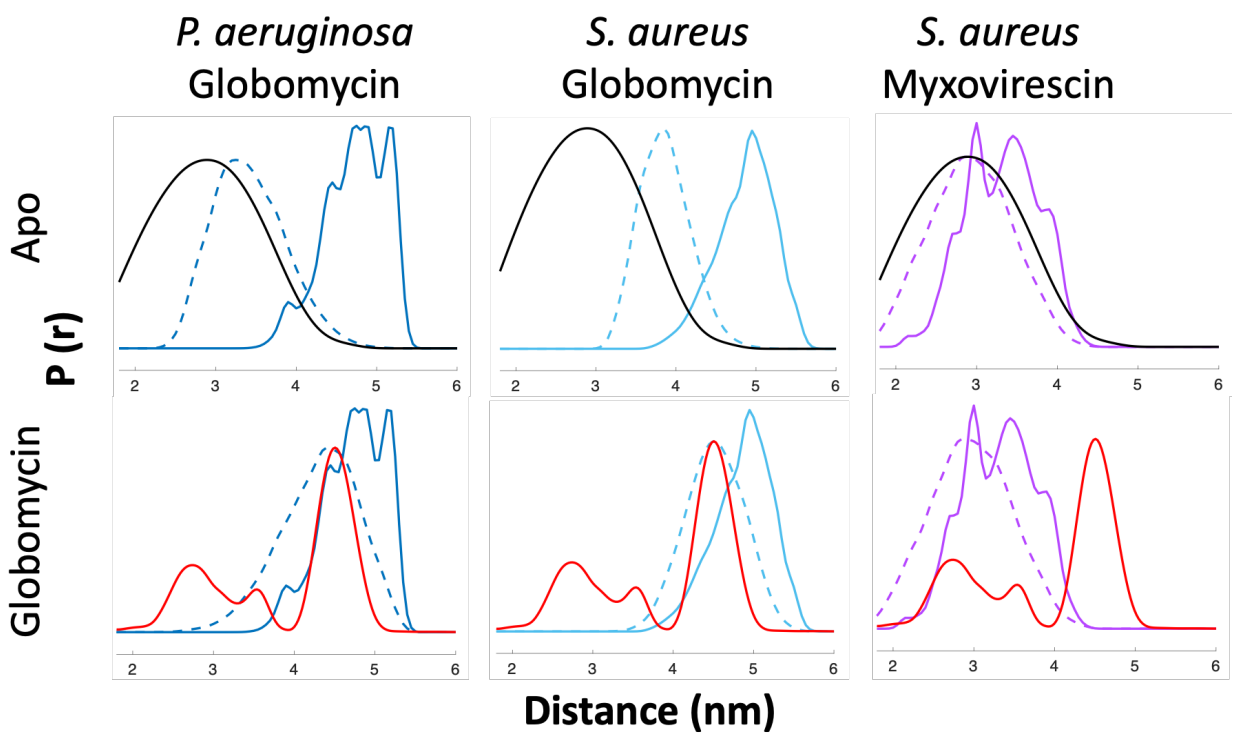

Figure S9. I43R1/A63R1 LspA MMM predicted spectra. MMM predicted spectra (solid lines) for *P. aeruginosa* globomycin bound structure (teal, left, PDB ID 5DIR), *S. aureus* globomycin bound structure (blue, middle, PDB ID 6RYO), and *S. aureus* myxovirescin bound structure (purple, right, PDB ID 6RYP), were compared and rotamer optimized (dashed lines) to fit to experimental apo (top, black) and globomycin bound (bottom, red) I43R1/A63R1 DEER data in FC12 micelles. Predicted spectra with no rotamer selection are shown as solid lines while rotamer optimized fits to experimental distance distributions are shown as dashed lines. I43R1/A63R1 corresponds to I41R1/S61R1 in *S. aureus* LspA. Rotamer optimized fits to the globomycin DEER data are broadened because MMM is trying to fit all populations rather than individual populations (Figure S8).

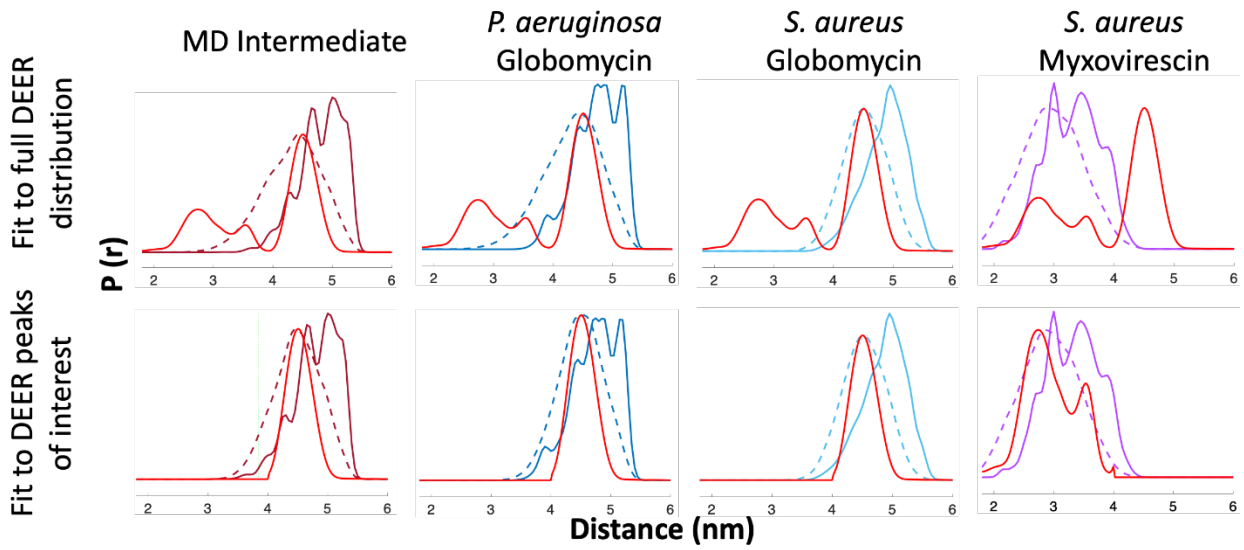

Figure S10. Rotamer optimized fits (dashed lines) to the globomycin DEER data (red) are broadened (top row, from Figure 3C and S7) because MMM attempts to fit all distance populations rather than individual populations (bottom row). When the rotamer optimization is performed against a selected population of the DEER data, the rotamer optimized MMM distributions fit better (bottom). The percentage of rotamers resulting in distances below 4 nm are only 3.6%, 5.4%, and 1.6% for the MD intermediate, LspPae in complex with globomycin (PDB 5DIR), and LspMrs in complex with globomycin (PDB 6RYO) structures, respectively. Similarly, only 4.5% of rotamers result in distances above 4 nm for the LspMrs in complex with myxovirescin (PDB 6RYP) structure. The fits and rotamer analysis strongly suggest that the globomycin bound structures agree with the longer distance peak seen in the DEER distribution while the myxovirescin structure agrees with the shorter distances seen in the DEER distribution.

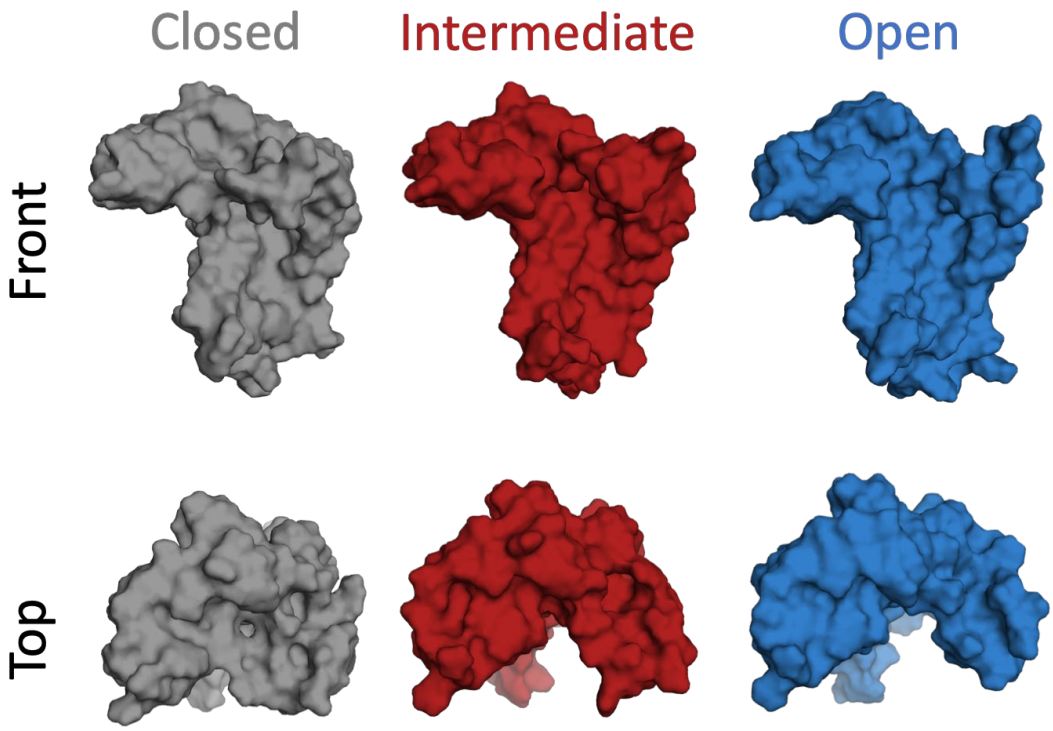

Figure S11. LspA conformational dynamics of the PH are observed in MD and EPR experiments. From the front view (top) and top view (bottom), the surface representations clearly show the opening of the active site from the closed (gray) to intermediate (maroon) to open (blue) conformations through the movement of the PH domain relative to the β-cradle. Colors and structures correspond to arrows in Figure 3A.

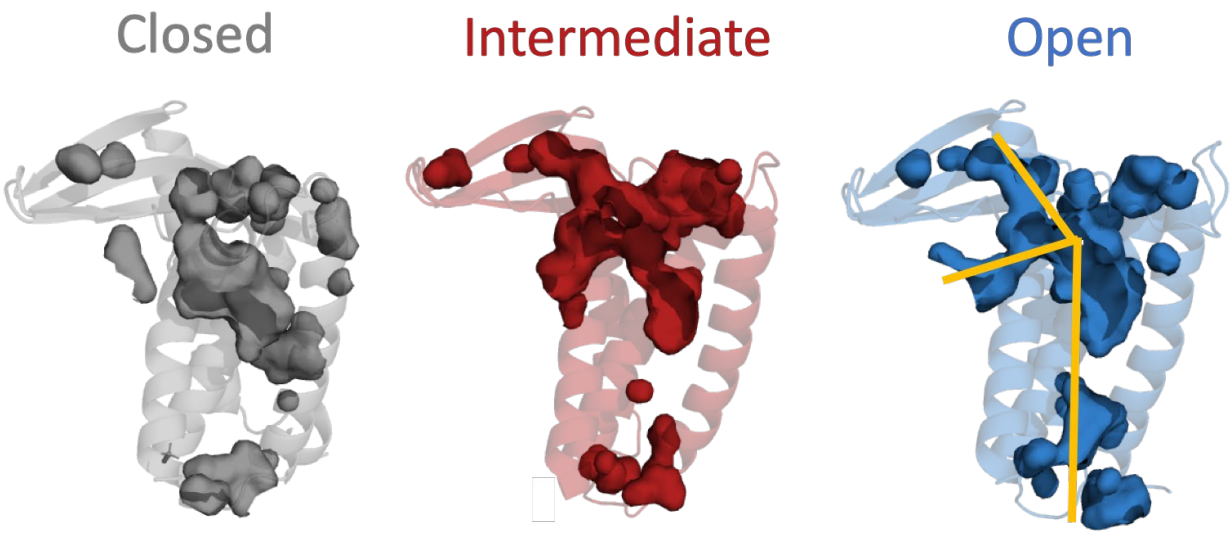

Figure S12. Cavity fill models generated in PyMOL show the space available in the active site and binding grooves. The trigonal cavity where the prelipoprotein is hypothesized to bind is most available in the open structure (right) and is shown as yellow lines.